Arch Appl Mech (2013) 83:207–223
DOI 10.1007/s00419-012-0647-z

ORIGINAL

A. S. Bouboulas · N. K. Anifantis

Three-dimensional finite element modeling of a vibrating beam with a breathing crack

Received: 6 September 2011 / Accepted: 8 May 2012 / Published online: 26 May 2012

Abstract This paper develops a full three-dimensional finite element model in order to study the vibrational behavior of a beam with a non-propagating surface crack. In this model, the breathing crack behavior is simulated as a full frictional contact problem between the crack surfaces, while the region around the crack is discretized into three-dimensional solid finite elements. The governing equations of this non-linear dynamic problem are solved by employing an incremental iterative procedure. The extracted response is analyzed utilizing either Fourier or continuous wavelet transforms to reveal the breathing crack effects. This study is applied to a cracked cantilever beam subjected to dynamic loading. The crack has an either uniform or non-uniform depth across the beam cross-section. For both crack cases, the vertical, horizontal, and axial beam vibrations are studied for various values of crack depth and position. Coupling between these beam vibration components is observed. Conclusions are extracted for the influence of crack characteristics such as geometry, depth, and position on the coupling of these beam vibration components. The accuracy of the results is verified through comparisons with results available from the literature.

Keywords Full three-dimensional · Finite element · Breathing crack · Frictional contact · Coupling

1 Introduction

Beams are fundamental members in numerous engineering structures and experience loading conditions, which may cause damages or cracks in overstressed zones. The presence of cracks in structural members, such as beams, induces local variations in stiffness, the magnitude of which depends on the position and depth of the cracks. These variations affect the vibrational behavior of the whole structure to a considerable degree. To ensure the safe and continuous operation of structures, it is important to detect any cracks in their members in a timely manner. Direct procedures, such as ultrasonic emission and X-radiography analysis, have been used for this purpose. However, these procedures have proven to be inoperative and unsuitable in certain cases, since they require expensive and time-consuming inspections [1]. To avoid these disadvantages, during the past decades, researchers have focused on more efficient procedures in crack detection using vibration-based methods [2]. Modeling of a crack is an important aspect of these methods.

Most previous studies assume that the crack in a structural member always remains open during vibration [3–7]. However, this assumption may not be valid when dynamic loadings are dominant. In this case, the crack breathes (opens and closes) regularly during vibration, inducing variations in the structural stiffness. These variations cause the structure to exhibit non-linear dynamic behavior [8]. The main distinctive feature of this

A. S. Bouboulas (✉) · N. K. Anifantis
Machine Design Laboratory, Mechanical and Aeronautics Engineering Department, University of Patras, 26500 Patras, Greece
E-mail: bouboula@otenet.gr

N. K. Anifantis
E-mail: nanif@mech.upatras.gr

behavior is the presence of higher harmonic components. In particular, a beam with a breathing crack shows natural frequencies between those of a non-cracked beam and those of a faulty beam with an open crack. Therefore, in these cases, vibration-based methods should employ breathing crack models to provide accurate conclusions regarding the state of damage. Several researchers [9–11] have developed breathing crack models considering only the fully open and fully closed crack states. However, experiments have indicated that the transition between these two crack states does not occur instantaneously [12]. Abraham and Brandon [13] represented the interaction forces between two segments of a beam, separated by a crack, using time-varying connection matrices. These matrices were expanded in Fourier series to simulate the alternation of a crack opening and closing. However, the implementation of this study requires excessive computer time. Douka et al. [14,15] considered a simple periodic function to model the time-varying stiffness of a beam. However, this model is limited to the fundamental mode, and thus, the equation of motion for the beam must be solved.

A realistic model of a breathing crack is difficult to create due to the lack of fundamental understanding about certain aspects of the breathing mechanism. This involves not only the identification of variables affecting the breathing crack behavior, but also issues for evaluating the structural dynamic response of the fractured material. It is also not yet entirely clear how partial closure interacts with key variables of the problem. The actual physical situation requires a model that accounts for the breathing mechanism and for the interaction between external loading and dynamic crack behavior. When crack contact occurs, the unknowns are the field singular behavior, the contact region, and the distribution of contact tractions on the closed region of the crack. The latter class of unknowns does not exist in the case without crack closure. This type of complicated deformation of crack surfaces constitutes a non-linear problem that is too difficult to be treated with classical analytical procedures. Thus, a suitable numerical implementation is required when partial crack closure occurs.

Nandi and Neogy [16] studied the plane problem of a beam with an edge crack subjected to a harmonic load. The crack was simulated as a frictionless contact problem between the crack surfaces. Andrieux and Varé [17] developed a lumped cracked beam model from the three-dimensional formulation of the general problem of elasticity with unilateral contact conditions on the crack lips. This model was applied in cracked rotors analysis so that flexion dominant loading to be investigated particularly. El Arem [18] completed this latter model by including the shearing effects in the constitutive equations of a cracked beam section in bi-axial flexure. Buezas et al. [19] dealt with crack detection in structural elements, utilizing a generic algorithm optimization method. The crack was modeled as a notch or a wedge with a unilateral contact model. Georgantzinos and Anifantis [20] studied the effect of the crack breathing mechanism on the time-variant flexibility due to the crack in a rotating shaft that considered quasi-static approximation. They simulated the breathing crack as a full frictional contact problem. Based on this breathing crack simulation, Bouboulas and Anifantis [21] presented a two-dimensional finite element model to study the vibrational behavior of a beam with a breathing crack.

This paper continues the previous work of the authors [21]. In particular, a full three-dimensional finite element model is constructed to study the vibrational behavior of a beam with a non-propagating transverse surface crack. The beam is discretized into three-dimensional solid finite elements, while the breathing crack is treated as a full frictional problem between the crack surfaces. This non-linear dynamic problem is solved using an incremental iterative procedure. The derived response is analyzed using either Fourier or continuous wavelet transforms to investigate the breathing crack effects. The proposed study is assessed for the case of a dynamically loaded cantilever beam with a crack of either uniform or non-uniform depth across the beam cross-section. The beam vertical, horizontal, and axial vibrations are extracted for both crack geometries and various values of crack depth and position. Conclusions are extracted for the effect of crack characteristics on the observed coupling of these beam vibration components. The accuracy of the results is demonstrated through comparisons with results available from the literature. Observations are made to determine the utility of this study in crack detection techniques.

2 Finite element procedure

In the following, a full three-dimensional beam model with a non-propagating transverse surface crack is discussed. The crack surfaces are assumed to be planar and smooth and the crack thickness negligible. The beam material properties are considered linear elastic and the displacements and strains are assumed to be small. The region around the crack is discretized into three-dimensional solid finite elements. The breathing crack behavior is simulated as a full frictional contact problem between the crack surfaces, which is an inherently non-linear problem. Any possible sliding is considered to obey Coulomb's law of friction, and penetration between contacting areas is not allowed. The beam undergoes dynamic loading. The governing equations of this non-linear dynamic problem are solved utilizing an incremental iterative procedure. The extracted response

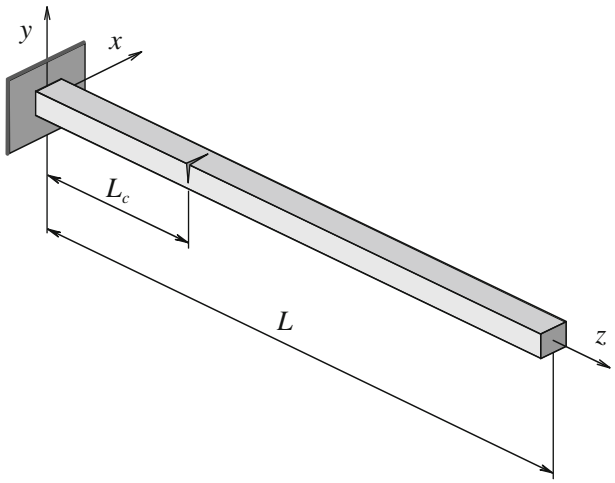

Fig. 1 Cracked beam model

is analyzed by employing either Fourier or continuous wavelet transforms. Although the incremental iterative procedure utilized, contact analysis and Fourier and continuous wavelet transforms are widely known, they are briefly discussed below for reasons of completeness.

Figure 1 illustrates a Euler-type three-dimensional straight cantilever beam with a rectangular cross-section $b \times h$ and length L. A breathing crack of two different geometries exists at position L_c. The crack has either a uniform depth a over the x-axis of the global Cartesian coordinate system x, y, z or a non-uniform depth varying linearly from a value of a_y at the plane $x = -b/2$ to a zero value at a distance a_x over the x-axis (Fig. 2). The morphology of the model is designed in a way that allows for changes in crack characteristics such as geometry, depth, and position. Thus, results can be extracted for various values of crack characteristics. A dynamic load is applied to the free end of the beam, acting over the y-axis and downward. The beam is discretized into finite elements, while the breathing crack behavior is simulated as a full frictional contact problem between the crack surfaces. Figure 3 shows the finite element meshes of a beam with a uniform and non-uniform depth crack. For both crack geometries, the beam is discretized into eight-node isoparametric hexahedral finite elements. Each node of such an element has three degrees of freedom that represent nodal displacements along the three dimensions. This model allows mesh refinement in the vicinity of the crack. Similar finite element meshes were developed for all of the crack cases considered in this study.

The crack is composed of two surfaces, which intersect on the crack front. Parts of these two surfaces may come into contact on an interface. The size of the interface can vary during the interaction between the load and the structure, but the interface is usually comprised of two parts, that is, an adhesive part and a slipping part, depending on the friction conditions maintained between the contacting surfaces. In the open crack state, the corresponding part of the crack surface is subjected to traction-free conditions. The so-called slave–master concept that is widely used for the implementation of contact analysis is adopted in this work for prediction of the crack-surface interference. One of the two crack surfaces is considered as the master surface, with the other as the slave. Both master and slave crack surfaces are defined by the local coordinate systems $({}^{\mathrm{J}}x_1, {}^{\mathrm{J}}x_2, {}^{\mathrm{J}}x_3)$, with J = I for master surface and J = II for slave surface. The axes ${}^{\mathrm{J}}x_3$ define the direction of the unit outward normal vector of the corresponding surfaces. The nodes that belong to the master and slave surfaces are called the master and slave nodes, respectively. Contact segments that span master nodes cover the contact surface of the structure. Therefore, the above problem can be regarded as contact between a slave node and a point on a master segment. This point may be located at a node, an edge, or a point of a master segment. A slave node makes contact with only one point on the master segment, but one master segment can make contact with one or more slave nodes at each time. For each contact pair, the mechanical contact conditions are expressed in a local coordinate system in the direction of the average normal to the boundaries of the bodies. Symbols u_i and R_i, $i = 1, 2, 3$ denote nodal displacement and force components, respectively, defined on the local coordinate systems $({}^{\mathrm{J}}x_1, {}^{\mathrm{J}}x_2, {}^{\mathrm{J}}x_3)$, J = I, II. The subscripts that indicate nodal numbers are dropped for simplicity from this point forward.

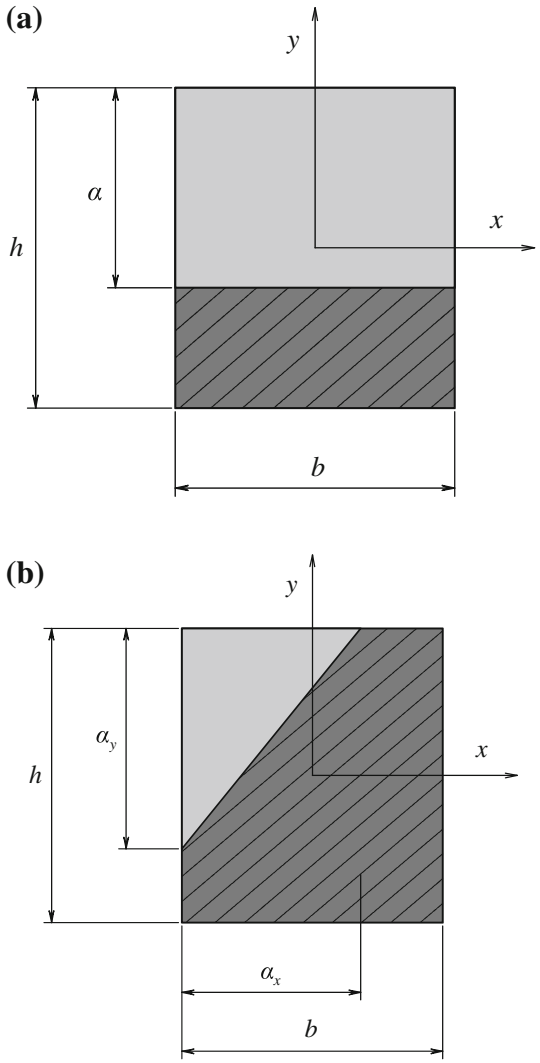

Fig. 2 Geometry of a crack with **a** uniform and **b** non-uniform depth

Recalling the equilibrium condition, the force between the components is always expressed by the following equations:

$$^{\mathrm{I}}R_i + {}^{\mathrm{II}}R_i = 0, \quad i = 1, 2, 3. \tag{1}$$

In the open crack state, the following traction-free conditions are held between the components:

$$^{\mathrm{I}}R_i = {}^{\mathrm{II}}R_i = 0, \quad i = 1, 2, 3. \tag{2}$$

From the definition of adhesion, the displacement components on the corresponding crack surfaces are interconnected by the equations:

$$^{\mathrm{I}}u_i + {}^{\mathrm{II}}u_i = 0, \quad i = 1, 2. \tag{3}$$

When an initial gap g^0 exists in the normal direction between the master and slave nodes of the corresponding node pair, the displacement component along the normal direction is:

$$^{\mathrm{I}}u_3 + {}^{\mathrm{II}}u_3 = g^0. \tag{4}$$

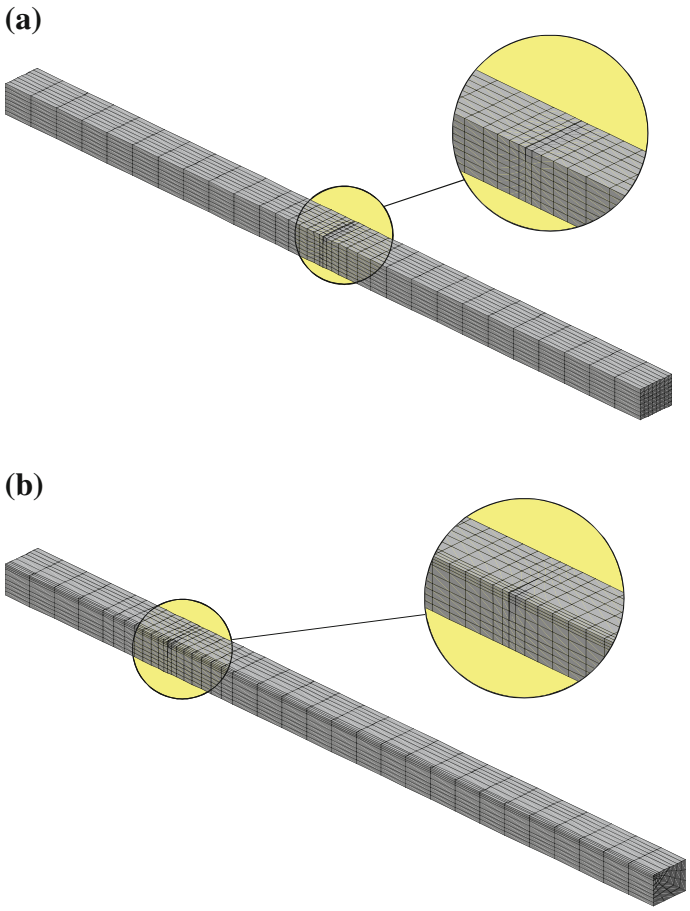

Fig. 3 Finite element mesh of a beam with **a** a crack of uniform depth $a/h = 0.25$ at position $L_c/L = 0.5$ or **b** a crack of non-uniform depth $a/h = 0.5$ at position $L_c/L = 0.25$

The slip state does not prohibit the existence of a gap between the crack surfaces, so Eq. (4) is still valid in this case. However, the tangential force component is defined in terms of friction as:

$$^{\mathrm{I}}R_i \pm \mu\, ^{\mathrm{I}}R_3 = 0, \quad i = 1, 2 \tag{5}$$

where μ is the coefficient of Coulomb friction. Equation (5) shows that the tangential force components are proportional to the normal component. In this sense, the movement in equal scale is prevented even as the displacement in one tangential direction is small comparing to the displacement in the second one. However, Eq. (5) constitutes a first estimation of the tangential force components and it is applied only in the first iteration of the iterative procedure described below. Better approximations are obtained in the subsequent iterations. Based on this procedure, the obtained tangential force and displacement components are compatible.

In the finite element method (FEM) framework, the finite element equilibrium equations governing the non-linear dynamic behavior of the three-dimensional beam are:

$$\mathbf{M}\ddot{\mathbf{U}} + \mathbf{C}\dot{\mathbf{U}} + \mathbf{K}\mathbf{U} = \mathbf{R}, \tag{6}$$

where **M**, **C** and **K** denote the mass, damping, and stiffness matrices, respectively. The time-dependent vectors $\ddot{\mathbf{U}}$, $\dot{\mathbf{U}}$, **U** and **R** are the nodal accelerations, velocities, displacements, and external forces, respectively, in terms of the global Cartesian coordinate system x, y, z.

The non-linear equations (6) are solved using an implicit direct integration scheme [22]. Based on this method, the time solution under consideration, T, is subdivided into N equal time increments $\Delta t = T/N$. Approximate solutions of Eq. (6) are sought at times $0, \Delta t, 2\Delta t, \ldots, t, t + \Delta t, \ldots, T$. Assuming that the solutions at times $0, \Delta t, 2\Delta t, \ldots, t$ are known, the solution at the next time increment, $t + \Delta t$, is acquired

by utilizing the modified Newton–Raphson iteration method. Thus, Eq. (6) is evaluated at time $t + \Delta t$ and iteration k as [21,22]:

$$ {}^{t}\mathbf{K}_T \ \Delta\mathbf{U}^{(k)} = \Delta\mathbf{R}^{(k-1)}, \tag{7} $$

with:

$$ {}^{t+\Delta t}\mathbf{U}^{(k)} = {}^{t+\Delta t}\mathbf{U}^{(k-1)} + \Delta\mathbf{U}^{(k)}, \tag{8} $$

where the left-hand subscripts denote the time, while the right-hand subscripts in brackets represent the iteration number, with $k = 1, 2, 3, \ldots$. The matrix ${}^{t}\mathbf{K}_T$ is a function of the tangent stiffness matrix, mass matrix, and damping matrix. The incremental nodal force vector $\Delta\mathbf{R}^{(k-1)}$ contains the nodal force vector and contributions from the inertia and damping of the system and the vector $\Delta\mathbf{U}^{(k)}$ contains the incremental nodal displacements. In each iteration, except the first, the most recent displacement estimates are used to calculate the vector $\Delta\mathbf{R}^{(k-1)}$ [22,23]. Then, the incremental displacements $\Delta\mathbf{U}^{(k)}$ are derived by solving Eq. (7), while the nodal displacements ${}^{t+\Delta t}\mathbf{U}^{(k)}$ are obtained from Eq. (8).

Considering that the problem has been solved for time t, and consequently, vectors ${}^{t}\mathbf{U}$ and ${}^{t}\mathbf{R}$ are known for the entire structure. To determine the corresponding displacement and forces vectors at time $t + \Delta t$, the Eqs. (1)–(5) are written in incremental form as following:

$$ {}^{t+\Delta t}\left({}^{\mathrm{I}}\Delta R_i\right) + {}^{t+\Delta t}\left({}^{\mathrm{II}}\Delta R_i\right) = 0, \quad i = 1, 2, 3 \tag{9} $$

$$ {}^{t+\Delta t}\left({}^{\mathrm{I}}\Delta R_i\right) = -{}^{t}\left({}^{\mathrm{II}}R_i\right), \quad i = 1, 2, 3 \tag{10} $$

$$ {}^{t}\left({}^{\mathrm{I}}u_i\right) + {}^{t+\Delta t}\left({}^{\mathrm{I}}\Delta u_i\right) = {}^{t}\left({}^{\mathrm{II}}u_i\right) + {}^{t+\Delta t}\left({}^{\mathrm{II}}\Delta u_i\right), \quad i = 1, 2 \tag{11} $$

$$ {}^{t}\left({}^{\mathrm{I}}u_3\right) + {}^{t+\Delta t}\left({}^{\mathrm{I}}\Delta u_3\right) = {}^{t}\left({}^{\mathrm{II}}u_3\right) + {}^{t+\Delta t}\left({}^{\mathrm{II}}\Delta u_3\right) - g^0, \tag{12} $$

$$ {}^{t}\left({}^{\mathrm{I}}R_i\right) + {}^{t+\Delta t}\left({}^{\mathrm{I}}\Delta R_i\right) = \pm\mu\left({}^{t}\left({}^{\mathrm{I}}R_3\right) + {}^{t+\Delta t}\left({}^{\mathrm{I}}\Delta R_3\right)\right). \quad i = 1, 2 \tag{13} $$

For reasons of simplicity, the iteration number has been omitted from Eqs. (9)–(13). However, the formulation given below is repeated for all iterations. These equations are transformed to the global Cartesian coordinate system x, y, z and are then embedded and rearranged into Eq. (7). To determine the corresponding nodal displacements at time $t + \Delta t$, the contact conditions must first be satisfied. Therefore, the iterative procedure employed must be applied by initially using the convergent contact status (union of the adhesive, slipping, and open parts of the crack surface) of the previous time t. The procedure initially assumes that the coplanar and normal incremental force components for a master surface at time $t + \Delta t$ are zero. Accurate values of the incremental forces can be estimated via the iterative procedure [22,23]. The contact state for each node pair is examined using criteria that check whether any violations related to geometrical compatibility and force continuity have occurred [20,21]. Where necessary, appropriate changes from open to contact or from adhesion to slip states and vice versa are made to identify the equilibrium state of the contact conditions. The new contact condition is applied to the node pair closest to the change. If the change is from the open to the contact state, then the adhesion condition is adjusted. When the iterative procedure converges, the incremental nodal values ${}^{t+\Delta t}\Delta\mathbf{U}$ and ${}^{t+\Delta t}\Delta\mathbf{R}$ are known for the entire structure. After calculating the total nodal values, the procedure goes to the next step of the time increment and continues until the final time increment is reached. The problem solution is then attained.

In order to simplify the computation, conditions associated with the partial closing and opening of the crack surfaces were modeled through the slideline facility of the Lusas commercial finite element code [23]. Slidelines were comprised of two necessarily non-regular surfaces defined by a number of contact segments corresponding to the external faces of elements closest to the surfaces. The nodal constraint treatment allows for the adjustment of contact conditions by setting appropriate constraints. At each increment of the procedure, this facility tracks the node pairs that are nearly in contact and adjusts the contact constraints. This technique does not directly couple the nodal degrees of freedom, but instead introduces repellent forces between the penetrating regions of the two surfaces. Coupling the nodal freedoms in this manner introduces no additional equations into the solution, and the technique is sufficiently flexible to be implemented within both explicit and implicit types of finite element codes.

3 Response analysis

The response extracted from the previously described finite element procedure cannot be examined directly to distinguish the breathing crack effects. For this reason, fast Fourier and continuous wavelet transforms are employed. These two popular transforms in signal analysis are briefly discussed below for reasons of completeness, and more information can be found in references [24,25].

The fast Fourier transform (FFT) is a perfect tool for finding the frequency components in a signal of stationary nature. Unfortunately, FFT cannot show the time point at which a particular frequency component occurs. Therefore, FFT is not a suitable tool for a non-stationary signal, such as the impulsive response of the cracked cantilever beam considered in this study, which requires time-frequency representation. To overcome this FFT deficiency, the short time Fourier transform (STFT) could be adopted, which maps a signal into a two-dimensional function of time and frequency. This windowing technique analyzes only a small section of the signal at a time. However, the information about time and frequency that is obtained has a limited precision that is determined by the size of the window, which is the same for all frequencies.

Wavelet transforms are a novel and precise way to analyze signals and can overcome the problems that other signal transforms exhibit. The most important advantage of wavelet transformations is that they have changeable window dimensions. For low frequencies, the window is wide, while for high frequencies, it is narrow. Thus, maximum time frequency resolution is provided for all frequency intervals.

The continuous wavelet transform (CWT), as employed in this study, is defined mathematically as:

$$Wf_{s,u} = \frac{1}{\sqrt{s}} \int_{-\infty}^{\infty} f(t)\psi^* \left(\frac{t-u}{s} \right) \mathrm{d}t, \tag{14}$$

where $f(t)$ is the signal for analysis, $\psi^*(t)$ is the complex conjugate of the mother wavelet $\psi(t)$, and s and u are real-valued parameters used to characterize the dilation and translation features of the wavelet.

The CWT has an inverse that permits recovery of the signal from its coefficient $Wf_{s,u}$ and is defined as:

$$f(t) = \frac{1}{C_\psi} \int_{-\infty}^{\infty} \int_{-\infty}^{\infty} Wf_{s,u}\psi \left(\frac{t-u}{s} \right) \frac{1}{s^2} \mathrm{d}s\mathrm{d}u, \tag{15}$$

where C_ψ is a constant depending on the wavelet type.

4 Numerical results and discussions

In this section, the presented method is applied for the cracked cantilever beam model shown in Fig. 1. This three-dimensional model has length $L = 2\,m$, cross-section $b \times h = 1 \times 10^{-4}\mathrm{m}^2$, modulus of elasticity $E = 2.06 \times 10^{11}$ Pa, mass density $\rho = 7800\,\mathrm{kg/m}^3$, and Poisson's ratio $\nu = 0.3$. For reasons of comparison and calculation simplicity, the two parameters describing the geometry for a non-uniform depth crack are considered equal to the parameter representing the geometry of a uniform depth crack, that is, $a_x = a_y = a$. For both crack geometries, the beam vibrational behavior is studied for various values of dimensionless depth a/h and position L_c/L. Throughout this study, generally moderate and high values of dimensionless crack depth ($a/h \geq 0.125$) are considered, since vibration-based crack detection methods are only slightly sensitive to small cracks [26]. A downward and vertical (y-axis) impulse loading is applied at the free end of the beam from time $t = 0$ to $t = \Delta t$. As previously mentioned, the beam is discretized into eight-node isoparametric hexahedral finite elements. Two typical meshes are illustrated in Fig. 3: the first mesh corresponds to a beam with a uniform depth crack of $a/h = 0.25$ at position $L_c/L = 0.5$ and the second mesh corresponds to a beam with a non-uniform depth crack of $a/h = 0.5$ at position $L_c/L = 0.25$. For all crack cases in this study, the beam finite element meshes are composed of approximately the same number of nodes and elements. For example, when the beam contains a uniform depth crack of $a/h = 0.25$ at position $L_c/L = 0.5$, the finite element mesh consists of 2,176 eight-node isoparametric hexahedral finite elements and 2,853 nodes. For the non-cracked beam, the finite element mesh is composed of 2,048 eight-node isoparametric hexahedral finite elements and 2,673 nodes. Convergence studies show that higher mesh refinements in the neighborhood of the crack affect the results less than 1.5 % for all studied cases. The non-linear dynamic problem is solved

by utilizing the finite element procedure presented above. The damping loss factor is very small for the carbon steel beam specimens considered in this study. Furthermore, in the modal analysis performed below, the damping loss factor only affects the amplitude of the response. For these reasons, the damping effects are neglected ($\mathbf{C} \approx \mathbf{0}$). At time zero ($t = 0$), the beam is stationary and un-deformed. The implicit Newmark time integration scheme is adopted in this finite element procedure with $\delta = 1/2$ and $\alpha = 1/4$ [22]. The considered time solution is subdivided into $N = 2^{11}$ equal time increments. Based on convergence studies, the time increment is taken as $\Delta t = 1 \times 10^{-4}$. The use of smaller values of time increments affects the results by less than 1.5 %. Numerical experimentations show that, for the smooth crack surfaces considered, the results are not significantly affected by the values of the coefficient of friction (less than 0.5 %). Hence, the results presented in the following for a small friction coefficient ($\mu = 0.1$) should be reasonably unaffected for most of the studied cases. Equation (7) is solved repeatedly until the contact status converges and the incremental displacements are sufficiently small. Generally, only a few iterations (no more than three) are needed between two subsequent sequences. This is reasonable, since the crack surfaces are small and the finite element mesh around the crack is dense. This problem is implemented utilizing the Lusas finite element commercial code [23]. The output files of this code are large, the handling of which demands parallel computers with multiple processing and memory units. Furthermore, conventional finite element programs need to be re-designed in order to take full advantage of parallel computers. For this reason, the response for the first $N = 500$ time increments is analyzed using FFT and CWT. The FFT is employed to find the frequency content of the response, since an eigenvalue analysis is only applicable to linear dynamic models. Unfortunately, the FFT causes the time information to be lost for a non-stationary signal such as the impulse response of the crack cantilever beam model. CWT is employed to overcome this deficiency, which provides the time–frequency information of a signal and enables the extraction of features that vary with time. Trial and error show that the Hanning window is suitable for FFT, while the biorthogonal 6.8 wavelet family is appropriate for CWT. For reasons of accuracy, the linear dynamic problem of a beam with a continuously open crack is considered. This problem is solved by employing the above finite element procedure without considering the contact equations described above. The eigenvalue analysis of non-cracked and open cracked beams is also considered for the same reasons. These problems are solved utilizing conventional finite element procedures [22]. Finally, conclusions are extracted for the utility of this study in crack detection techniques. An accuracy study is implemented for the non-cracked beam. The first four analytical natural frequencies f_{iu} of the beam are considered [27]. The subscripts $i = 1, 2, 3, 4$ represent the order of the natural frequency, while u denotes the non-cracked state of the beam. The first two natural frequencies are identical, $f_{1u} = f_{2u} = 0.209$ kHz, and correspond to the first bending vibration in the horizontal $(x - z)$ and vertical $(y - z)$ planes, respectively. The last two natural frequencies are also identical, $f_{3u} = f_{4u} = 1.31$ kHz, and correspond to the second bending vibration in the horizontal $(x - z)$ and vertical $(y - z)$ planes, respectively. Comparisons are performed with the corresponding numerical natural frequencies f_{iu}^* obtained by the eigenvalue finite element procedure, where $*$ denotes the numerical results. The percentage differences $((f_{iu} - f_{iu}^*)/f_{iu}^*) \times 100$ of these natural frequencies are between 0.27 % for the first natural frequency and 0.72 % for the fourth natural frequency. Thus, the analytical and numerical results are very close. An accuracy study is also implemented by employing the numerical results f_{iu}^*, which are the natural bending frequencies extracted from the FFT of the corresponding displacement response. Comparisons are performed with the analytical natural frequencies f_{iu} noted above. The percentage differences of these natural frequencies are between 0.56 and 2.35 % for the first and fourth natural frequencies, respectively. Thus, the results obtained using the FFT are very close to the analytical values. Comparisons with the previous study show that the accuracy of the natural frequencies obtained with the eigenvalue finite element procedure is higher than that obtained with the FFT. An accuracy study is also implemented for a beam with an open crack of uniform depth $a/h = 0.5$ at position $L_c/L = 0.5$. The first four natural frequencies are obtained based on the FFT of the vertical and horizontal displacement responses. These results are compared with the corresponding natural frequencies extracted from the eigenvalue finite element procedure. The percentage differences of the first four natural bending frequencies are between 0.17 and 4.2 % for the first and fourth natural frequencies, respectively. To obtain a first insight into the cracked beam vibrational behavior, an eigenvalue analysis is performed considering the crack always open. The breathing crack approach is not employed, since it introduces non-linearities that make the eigenvalue analysis inapplicable. However, there are instances during the beam free vibration at which the breathing crack is open. Based on the deformed mesh of the employed eigenvalue finite element procedure, the vibration modes of the beam are extracted for both crack geometries and for various values of crack depth and position. Coupled vibration modes are observed for all crack cases considered. For example, Fig. 4 depicts the two different coupled vibration modes of the beam with a uniform depth crack of $a/h = 0.5$ at position $L_c/L = 0.5$. The un-deformed shape of the beam

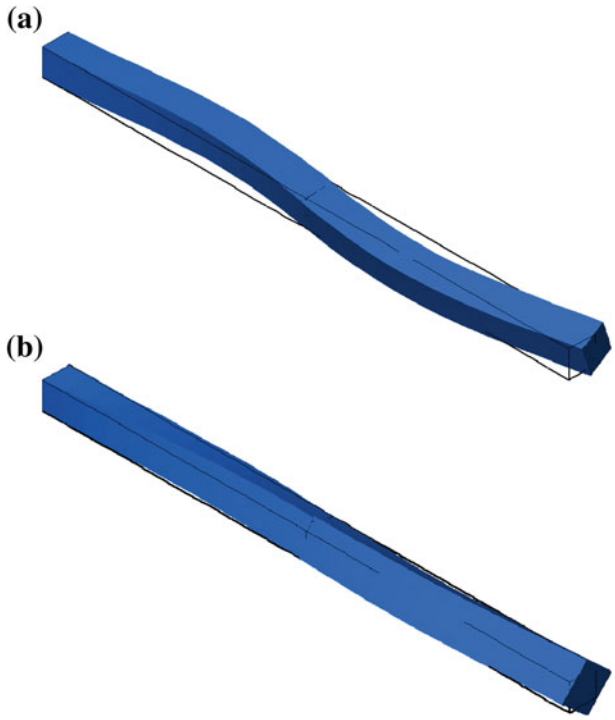

Fig. 4 Coupled bending-torsion vibration modes for the beam with an always open uniform depth crack of $a/h = 0.5$ at position $L_c/L = 0.5$ with **a** untwisted, or **b** twisted crack surfaces

(solid lines) is also shown in this figure for comparison. It seems that these two vibration modes result from coupling between the bending and torsion vibration modes. In these two vibration modes, the crack surfaces are either untwisted along the z-axis and exactly facing each other or twisted along the z-axis (Fig. 4). Figure 5 illustrates the two different coupled vibration modes of the beam with a non-uniform depth crack of $a/h = 1$ at position $L_c/L = 0.25$. These two modes derive from coupling of the longitudinal and torsion vibration modes or coupling between the bending and torsion vibration modes. The crack surfaces in these two coupled vibration modes are either untwisted along the z-axis and exactly facing each other or twisted along the z-axis, as in the case of a uniform depth crack (Fig. 5a).

Figure 6 illustrates the impulsive displacement response in the horizontal (x-axis), vertical (y-axis), and axial (z-axis) directions versus response time for the beam with an either uniform or non-uniform depth breathing crack of $a/h = 0.5$ at position $L_c/L = 0.25$. For reasons of visibility, the horizontal response for the uniform depth crack is magnified by a scale of 10^3 (Fig. 6a). It seems that for both crack cases the amplitude of the vertical vibration is greater than the corresponding amplitudes of the horizontal and axial vibrations. This is reasonable, since the cracked beam is excited along the vertical direction. A comparison between Fig. 6a, b shows that the crack geometry affects the amplitudes of the vibration components. The most significant change is observed in the amplitude of the horizontal vibration. In particular, the amplitude of the horizontal vibration for the non-uniform depth crack is much greater than the amplitude of the horizontal vibration for the uniform depth crack. Thus, the non-uniform depth crack causes more intense coupling than the uniform depth crack.

To get more insight into the cracked beam vibrational behavior, Fig. 7 depicts the instantaneous deformed shape for a beam with a uniform depth crack of $a/h = 0.75$ at position $L_c/L = 0.25$ when the crack is partially closed. Apart from the instantaneous deformed shape of the fractured beam, Fig. 7 also illustrates the un-deformed shape of the non-cracked beam for comparison and a detail showing the crack state. The displacements in the detail are magnified by a scale of 2. It seems that the beam vibrates like a two-dimensional structure. This happens due to the geometric symmetry of the crack surfaces in respect to the direction of the excitation. Figure 8 shows the instantaneous deformed shape for a beam with a non-uniform depth crack of $a/h = 1$ at position $L_c/L = 0.25$ when the crack is partially closed. It is seems that the geometric asymmetry of the crack surfaces in respect to the direction of the excitation causes coupling between transverse bending and torsion (along the z-axis) vibration modes. It is observed from Fig. 9, showing a perspective view of the cracked beam, that the beam also undergoes bending over the horizontal direction. Based on Figs. 7, 8, and 9,

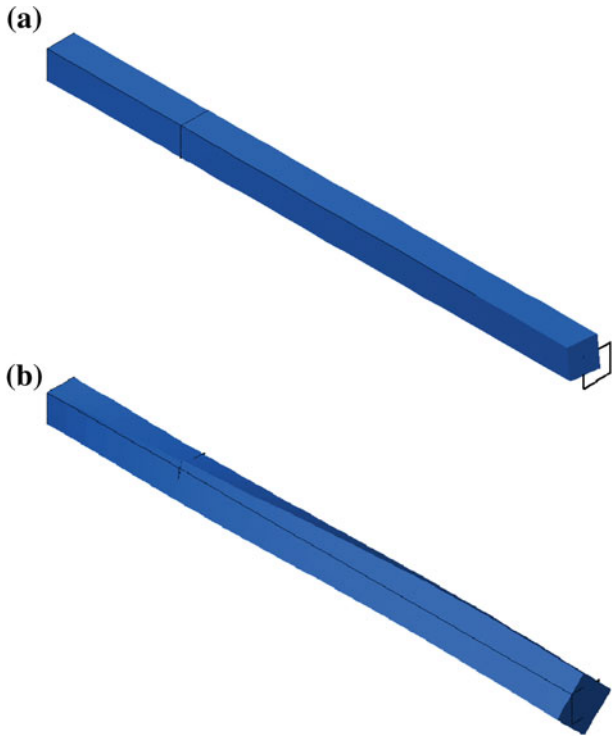

Fig. 5 Coupled **a** longitudinal-torsion (*untwisted crack surfaces*) **b** bending-torsion (*twisted crack surfaces*) vibration modes for the beam with an always open non-uniform depth crack of $a/h = 1$ at position $L_c/L = 0.25$

it is deduced that the non-uniform depth crack causes coupling between bending and torsion vibration modes. This coupling is un-steady due to the breathing crack effects. Furthermore, it seems that the portions of the beam on the left and right of the crack vibrate in different ways at the same time.

4.1 FFT analysis

Figure 10 depicts the FFTs of the horizontal, vertical, and axial acceleration response for a beam with either a uniform depth crack of $a/h = 0.5$ at position $L_c/L = 0.25$ or a non-uniform depth crack of $a/h = 0.5$ at position $L_c/L = 0.5$. In Fig. 10b, the axial response is magnified by a scale of 10 for visibility. Furthermore, the vertical dash-dot lines represent the frequency content of the non-cracked beam. In particular, the first line from the left represents the loci of the two identical natural frequencies for the first bending vibrations over the horizontal and vertical planes. The next dash-dot line represents the loci of the two identical natural frequencies for the second bending vibrations over the horizontal and vertical planes. These natural frequencies are evaluated from the FFT of the acceleration response, which is not plotted in this figure for clarity. For both crack cases, the first two primary peaks of the FFTs for the horizontal and vertical responses correspond to the first two bending vibrations over the horizontal and vertical planes, respectively. The remaining primary peaks of the illustrated FFTs in Fig. 10 are caused due to the coupled vibrations of the fractured beam, vibrations of the beam portions on the left and the right of the crack, and breathing crack effects. Identification of these frequencies requires more investigation, which is beyond the scope of this work. A comparison between Fig. 6a, b shows differences in the values of amplitudes. Although the value of the crack depth is the same for both crack cases, the values of amplitudes for the uniform depth crack are much greater than the corresponding values for the non-uniform depth crack. This is due to the different geometry of the cracks and not because of their different positions along the beam. The above study was implemented for both crack geometries and various values of crack depth and position. As expected [21], the natural frequencies decrease as the crack depth increases. Furthermore, the effect of the crack on the natural frequencies weakens as the distance between the crack and the cantilever end increases. The purpose of this study was to numerically simulate the breathing crack mechanism and its interaction with the vibrational behavior of a beam. Thus, the implementation of very expensive

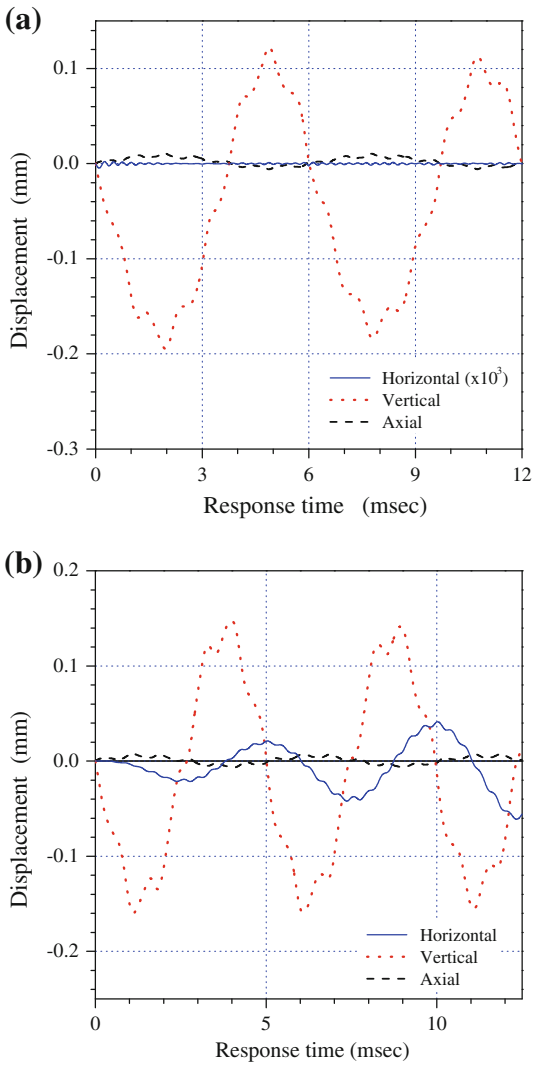

Fig. 6 Time response when a breathing crack with a **a** uniform depth or **b** non-uniform depth of $a/h = 0.5$ is present at position $L_c/L = 0.25$

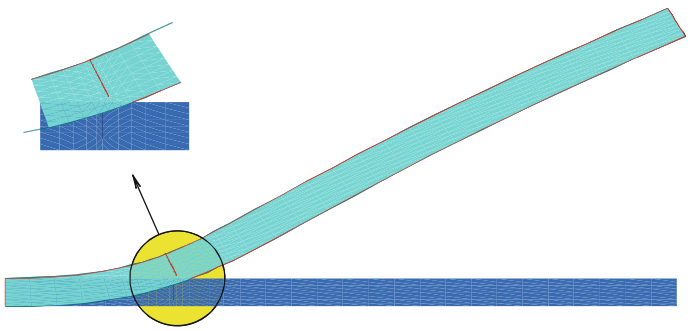

Fig. 7 Instantaneous deformed shape of a beam with a breathing crack of uniform depth $a/h = 0.75$ at position $L_c/L = 0.25$

and time-consuming experiments of a cantilever beam with a breathing crack is beyond the scope of this study. However, to validate the results of the present study, the behavior of the impulsive displacement response is considered. In comparison with the displacements of the open crack model, the displacement values for the breathing crack model are generally smaller. This is reasonable since the breathing of a crack causes changes

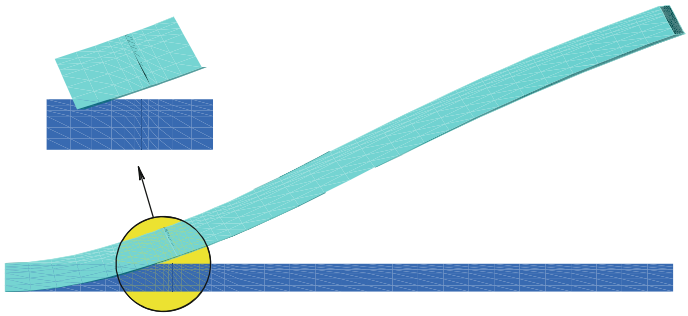

Fig. 8 Instantaneous deformed shape of a beam with a breathing crack of non-uniform depth $a/h = 1$ at position $L_c/L = 0.25$

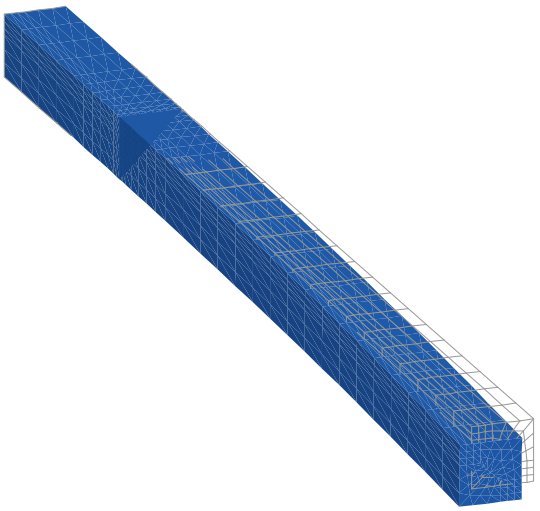

Fig. 9 Instantaneous deformed shape of a beam with a breathing crack of non-uniform depth $a/h = 1$ at position $L_c/L = 0.25$

in the structural stiffness during the response cycle. Similar conclusions are presented in reference [28]. In what follows, the accuracy of the presented study is shown through comparisons of the natural frequencies obtained from the FFT of the vertical acceleration response with the corresponding frequencies available from the literature. The FFT of the vertical accelerations is not given here, for brevity reasons. However, it is similar to those presented in Fig. 10. Herein, the dimensionless fundamental bending natural frequency over vertical direction of the cantilever beam, f_{1c}/f_{1u}, is evaluated for a uniform depth breathing crack with three different values of a/h at position $L_c/L = 0.25$. Subscript c denotes the cracked beam. The results of this study are illustrated in Fig. 11. For each value of the crack depth, the frequency range is presented by an error bar. The upper values of these bars correspond to the frequency for the fully closed crack state, while the lower values correspond to the frequency for the fully open crack state. Between the frequencies for fully closed and fully open crack lie the corresponding frequencies for always open crack [29]. To study further the accuracy of the presented study, the two lower bending natural frequencies over vertical direction of the cantilever beam with a breathing uniform depth crack of $a/h = 0.5$ at position $L_c/L = 0.5$ are evaluated (Table 1). It is derived from Table 1 that the results of the present study are generally close to the results of Nandwana and Maiti [30] and Kisa and Brandon [31]. It is noteworthy that the study of Nandwana and Maiti [30] has applied for a Timoshenko beam. Furthermore, the results from the work of Kisa and Brandon [31] correspond to an internal crack of the same severity with the studied crack case. The internal crack constitutes a good approximation of a fully closed crack.

4.2 CWT analysis

In this subchapter, the CWT is employed to investigate the effect of a breathing crack on the beam vibrational behavior. Three-dimensional contour maps of the CWTs for the impulsive displacements over three directions

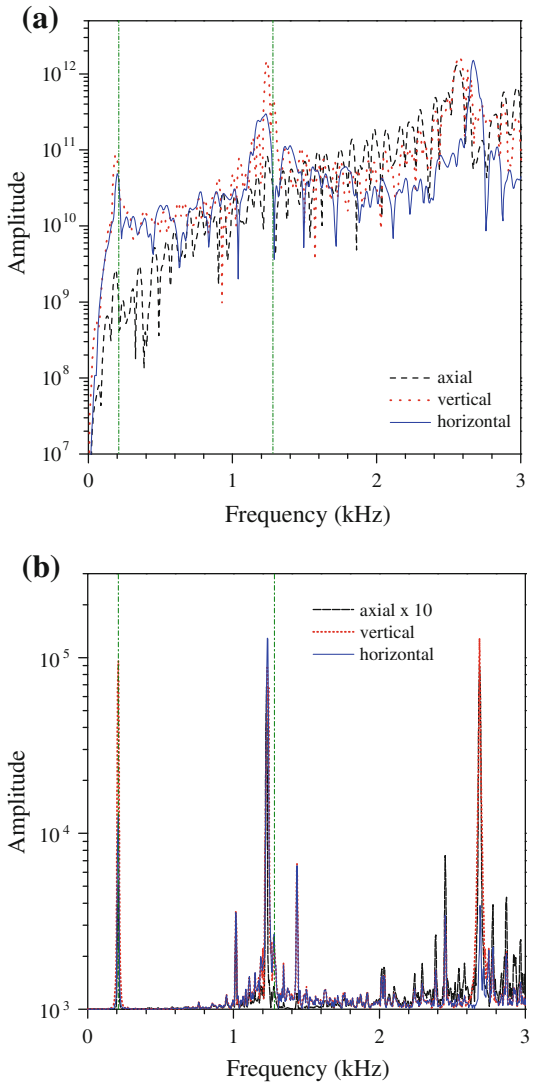

Fig. 10 Frequency response of the acceleration for **a** a uniform depth breathing crack of $a/h = 0.5$ at position $L_c/L = 0.25$ or **b** a non-uniform depth crack of $a/h = 0.5$ at position $L_c/L = 0.5$

are discussed for various crack scenarios. In these contour maps, the symbol s denotes the scale space, u stands for the time space, and $Wf_{s,u}$ represents the wavelet coefficients. The scale may conceptually be considered the inverse of the frequency. Though there is no exact mathematical relation for this, with approximation it can de stated as $f_a = f_c/s\Delta t$, where f_a is the pseudo frequency corresponding to scale s in kHz, f_c is the central frequency of the wavelet in kHz, and Δt is the time increment [32]. Based on this approximation, scales, and consequently pseudo frequencies, are correlated to the natural frequencies obtained by the corresponding FFT. Then, the values of the wavelet coefficients at these scales are determined from the contour maps for the entire time solution of interest. The contour maps presented below consist of two regions of different morphology and extent. In the first region, the map approaches the plane $s - u$ (nearly zero values of wavelet coefficients), while in the second (remaining) map region, the map consists of a number ridges. Figure 12a shows the contour map of the CWT for the impulsive vertical displacement response of a beam with a uniform depth crack of $a/h = 0.875$ at position $L_c/L = 0.5$. A number of vertical consecutive but non-uniform ridges is observed along scale axis and for $u \geq 200$. These ridges appear maximum values of wavelet coefficients at $s \approx 48 (f_a = 0.17\,\text{kHz})$ that corresponds to the first bending vibration over the vertical plane. The higher maximum value of wavelet coefficients, $Wf_{s,u} \approx 8 \times 10^7$, occurs at $s \approx 48$ and $u \approx 350$. Figure 12b illustrates a corresponding contour map of the horizontal response. For $u \geq 200$ and $s \leq 64$, the

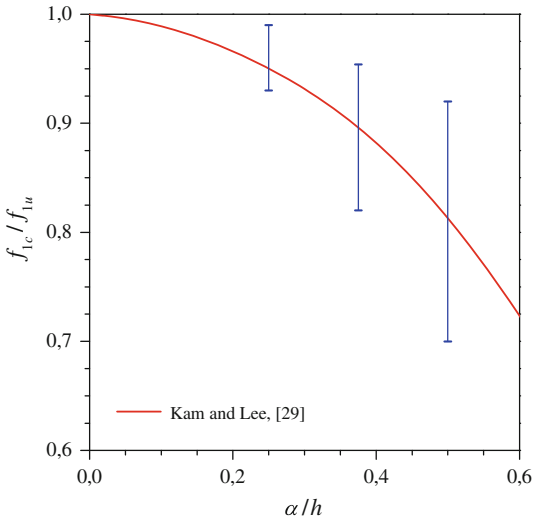

Fig. 11 Fundamental bending frequency over vertical direction of the cantilever beam with a uniform depth breathing crack of three different depths located at $L_c/L = 0.25$

Table 1 First two bending natural frequencies over vertical direction of the cantilever beam for a uniform depth crack of $a/h = 0.5$ at position $L_c/L = 0.5$

	f_{1c}/f_{1u}	f_{2c}/f_{2u}
Nandwana and Maiti [30]	1.000	0.992
Present study	0.992	0.957
% Difference of natural frequency	−0.80	−3.53
Kisa and Brandon [31]	0.980	0.925
Present study	0.992	0.957
% Difference of natural frequency	1.22	3.46

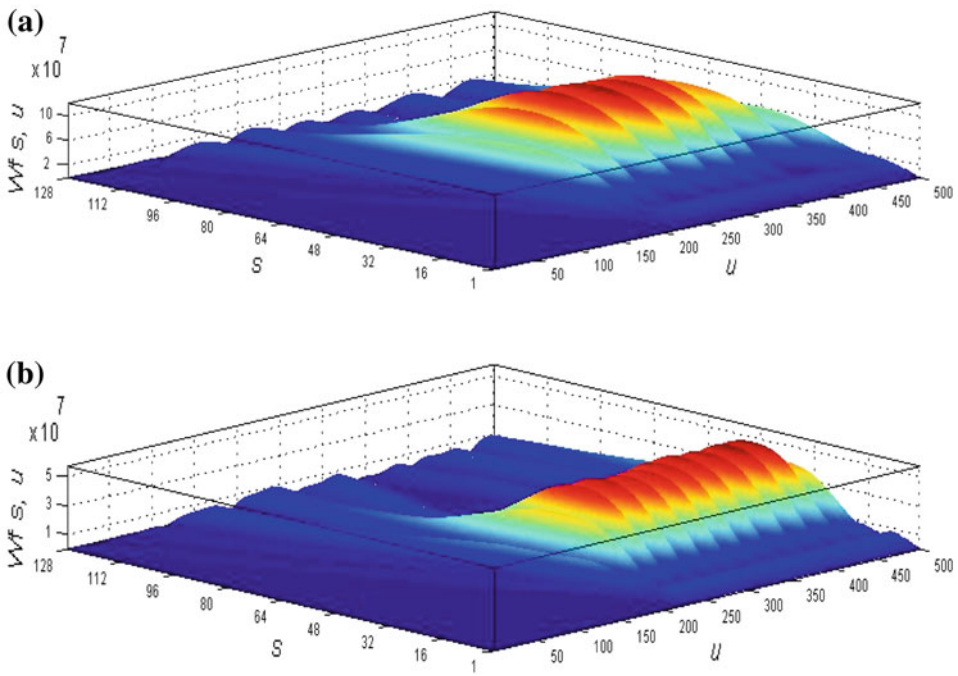

Fig. 12 CWT of the **a** vertical displacement and **a** horizontal displacement for a beam with a uniform depth breathing crack of $a/h = 0.875$ and $L_c/L = 0.5$

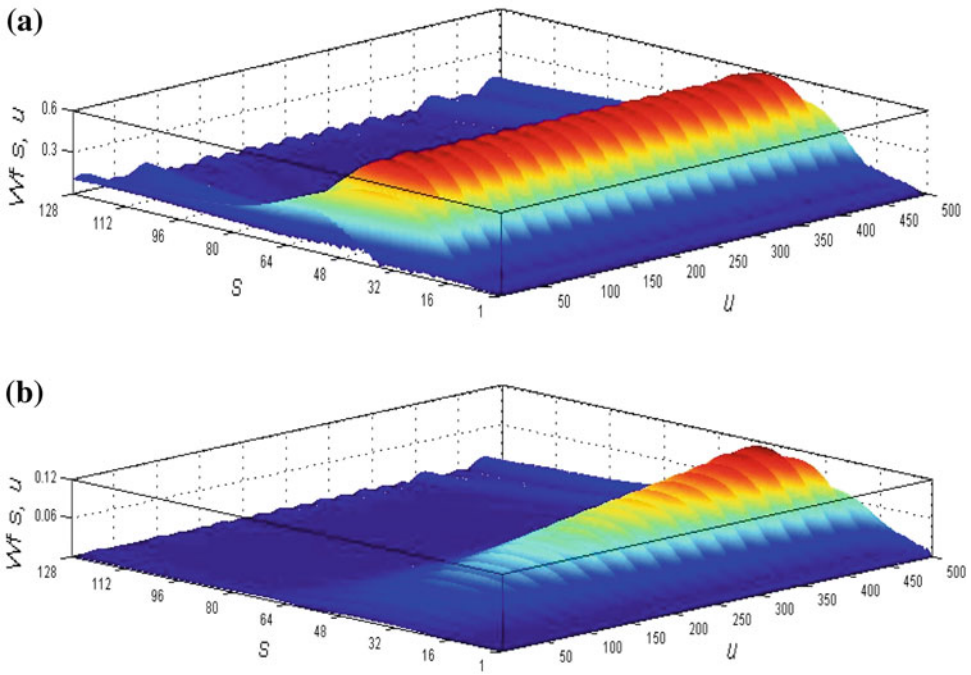

Fig. 13 CWT of the **a** vertical displacement and **b** horizontal displacement for a beam with a non-uniform depth breathing crack of $a/h = 0.5$ and $L_c/L = 0.25$

map consists of a number of vertical and nearly uniform ridges. The maximum values of wavelet coefficients, $Wf_{s,u} \approx 5 \times 10^7$, for these ridges are observed at $s \approx 32 (f_a = 0.25\,\text{kHz})$ which corresponds to the first bending vibration over the horizontal plane. Figure 13 shows the corresponding contour maps of the vertical and horizontal responses for a non-uniform depth crack of $a/h = 0.5$ at position $L_c/L = 0.25$. For the vertical response, a number of uniform ridges appear along time axis and for $s \leq 84$. The maximum wavelet coefficient value, $Wf_{s,u} \approx 0.6$, appears along $s \approx 42 (f_a = 0.19\,\text{kHz})$ corresponding to the first bending vibration over the vertical plane (Fig. 13a). For the horizontal response, a number of ridges are observed along time axis and for $s \leq 48$. The height of these ridges increases over the considered time. This happens because the response is in a transient state within the considered time. The maximum wavelet coefficient value $Wf_{s,u} \approx 0.12$ is observed at $s \approx 41 (f_a = 0.198\,\text{kHz})$ and $u = 450$. This later value of scale corresponds to the first bending vibration over horizontal plane. For both studied crack cases, the contour maps of the CWTs for the impulsive axial displacement response are not presented since similar conclusions to those for the vertical response are extracted. Furthermore, higher maximum values of the wavelet coefficients appear in the vertical directions than in the other two directions. This is reasonable, since the beam is excited along the vertical axis. Coupling of vibration components occurs in domain (s, u) at which the values of the wavelet coefficients of impulsive responses over three dimensions are simultaneously nonzero. The impulsive displacement responses over three directions were evaluated for different crack cases to investigate the effect of crack geometry, depth, and position on vibrational behavior using the CWT. Differences regarding the maximum values of the wavelet coefficients, the map morphology (the extent of the regions and shape of ridges), and the extent of coupling domain (s, u) are observed.

5 Conclusions

The work reported in this paper is part of ongoing research to develop precise crack detection techniques. In particular, a full three-dimensional finite element model was formulated to study the vibrational behavior of a beam with a breathing crack. This model was discretized into a number of conventional finite elements, while the breathing crack was treated as a full frictional contact problem between the crack surfaces. An iterative incremental procedure was applied to solve this non-linear problem. The derived time response was analyzed using various integral transforms including FFT and CWT. This study assessed an impulsive loading beam

with either a uniform or non-uniform depth crack. For both crack geometries, the beam vibrational behavior was investigated for various values of crack depth and position. The results of this study are in agreement with results available from the literature. Coupling between fundamental vibration modes is observed, which constitutes the main benefit of this full three-dimensional finite element model over a corresponding two-dimensional model. The coupling depends on the crack characteristics such as geometry, depth, and position. This analysis correlates the natural beam frequencies obtained by the FFT to the scales of contour maps. The values of the wavelet coefficients at these scales are determined from the contour maps for the time solution of interest. Thus, this study shows that FFT and CWT can be used as tools for crack detection techniques. These conclusions encourage the authors of this study to investigate the influence of more compound issues in vibration problems like plasticity and crack propagation. These issues are under investigation and will be the subject of future work for the authors.

References

1. Silva, J.M.M., Gomes, A.J.M.A.: Experimental dynamic analysis of cracked free–free beams. Exp. Mech. **30**, 20–25 (1990)
2. Doebling, S.W., Farrar, C.R., Prime, M.B., Shevitz, D.W.: A summary review of vibration based damage identification methods. Shock Vib. Dig. **30**, 91–105 (1998)
3. Christides, S., Barr, A.D.S.: One-dimensional theory of cracked Bernoulli–Euler beams. Int. J. Mech. Sci. **26**, 639–648 (1984)
4. Dimarogonas, A.D.: Vibration Engineering. West Publishers, St Paul (1976)
5. Chondros, T.G., Dimarogonas, A.D.: Identification of cracks in welded joints of complex structures. J. Sound Vib. **69**, 531–538 (1980)
6. Krawczuk, M., Żak, A., Ostachowicz, W.: Elastic beam finite element with a transverse elasto-plastic crack. Finite Elem. Anal. Des. **34**, 61–73 (2000)
7. Bouboulas, A.S., Anifantis, N.K.: Formulation of cracked beam element for analysis of fractured skeletal structures. Eng. Struct. **30**, 894–901 (2008)
8. Gudmundson, P.: The dynamic behavior of slender structures with cross-sectional cracks. J. Mech. Phys. Solids **31**, 329–345 (1983)
9. Cacciola, P., Muscolino, G.: Dynamic response of a rectangular beam with a known non-propagating crack of certain or uncertain depth. Comput. Struct. **80**, 2387–2396 (2002)
10. Benfratello, S., Cacciola, P., Impollonia, N., Masnata, A., Muscolino, G.: Numerical and experimental verification of a technique for locating a fatigue crack on beams vibrating under Gaussian excitation. Eng. Fract. Mech. **74**, 2992–3001 (2007)
11. Sholeh, K., Vafai, A., Kaveh, A.: Online detection of the breathing crack using an adaptive tracking technique. Acta Mech. **188**, 139–154 (2007)
12. Clark, R., Dover, W.D., Bond, L.J.: The effect of crack closure on the reliability of NDT predictions of crack size. NDT Int. **20**, 269–275 (1987)
13. Abraham, O.N.L., Brandon, J.A.: The modelling of the opening and closure of a crack. J. Vib. Acoust. **117**, 370–377 (1995)
14. Douka, E., Hadjileontiadis, L.J.: Time–frequency analysis of the free vibration response of a beam with a breathing crack. NDT&E Int. **38**, 3–10 (2005)
15. Loutridis, S., Douka, E., Hadjileontiadis, L.J.: Forced vibration behaviour and crack detection of cracked beams using instantaneous frequency. NDT&E Int. **38**, 411–419 (2005)
16. Nandi, A., Neogy, S.: Modelling of a beam with a breathing edge crack and some observations for crack detection. J. Vib. Control **8**, 673–693 (2002)
17. Andrieux, S., Varé, C.: A 3D cracked beam model with unilateral contact. Application to rotors. Eur. J. Mech. A/Solids **21**, 793–810 (2002)
18. El Arem, S.: Shearing effects on the breathing mechanism of a cracked beam section in bi-axial flexure. Eur. J. Mech. A/Solids **28**, 1079–1087 (2009)
19. Buezas, F.S., Rosales, M.B., Filipich, C.P.: Damage detection with genetic algorithms taking into account a crack contact model. Eng. Fract. Mech. **78**, 695–712 (2010)
20. Georgantzinos, S.K., Anifantis, N.K.: An insight into the breathing mechanism of a crack in a rotating shaft. J. Sound Vib. **318**, 279–295 (2008)
21. Bouboulas, A.S., Anifantis, N.K.: Finite element modeling of a vibrating beam with a breathing crack: observations on crack detection. Struct. Health Monit. **10**, 131–145 (2011)
22. Bathe, K.J.: Finite Element Procedures. Prentice-Hall, Upper Saddle River (1996)
23. LUSAS: *User Manual*. (FEA Ltd, England 2001)
24. Brigham, E.O.: The Fast Fourier Transform: An Introduction to Its Theory and Application. Prentice Hall, Englewood Cliffs (1973)
25. Rao, R.M., Bopardikar, A.S.: Wavelet Transforms—Introduction to Theory and Applications. Addison Wesley Longman, Reading (1998)
26. Dimarogonas, A.D.: Vibration of cracked structures: a state of the art review. Eng. Fract. Mech. **55**, 831–857 (1996)
27. Meirovitch, L.: Analytical Methods in Vibrations. The MacMillan Company, Collier MacMillan Limited, London (1967)
28. Qian, G.L., Gu, S.N., Jiang, J.S.: The dynamic behaviour and crack detection of a beam with a crack. J. Sound Vib. **138**, 233–243 (1990)
29. Kam, T.Y., Lee, T.Y.: Detection of cracks in structures using modal test data. Eng. Fract. Mech. **42**, 381–387 (1992)
30. Nandwana, B.P., Maiti, S.K.: Modelling of vibration of beam in presence of inclined edge or internal crack for its possible detection based on frequency measurements. Eng. Fract. Mech. **58**, 193–205 (1997)

31. Kisa, M., Brandon, J.: The effects of closure of cracks on the dynamics of a cracked cantilever beam. J. Sound Vib. **238**, 1–18 (2000)
32. Gangopadhyay, T.K., Chakravorti, S., Bhattacharya, K., Chatterjee, S.: Wavelet analysis of optical signal extracted from a non-contact fibre-optic vibration sensor using an extrinsic Fabry–Perot interferometer. Meas. Sci. Technol. **16**, 1075–1082 (2005)